Structural Characterization, Membrane Interaction, and Specific Assembly within Phospholipid Membranes of Hydrophobic Segments from *Bacillus thuringiensis* var. *israelensis* Cytolytic Toxin†

Ehud Gazit and Yechiel Shai*

Department of Membrane Research and Biophysics, Weizmann Institute of Science, Rehovot, 76100 Israel

Received May 4, 1993; Revised Manuscript Received September 3, 1993®

ABSTRACT: The *Bacillus thuringiensis* var. *israelensis* (Bti) cytolytic toxin is hypothesized to exert its toxic activity via pore formation in the cell membrane as a result of the aggregation of several monomers. To gain insight into the toxin's mode of action, 2 putative hydrophobic 22 amino acid peptides were synthesized and characterized spectroscopically and functionally. One peptide corresponded to the putative amphiphilic α-helical region (amino acids 110–131, termed helix-2), and the other to amino acids 50–71 (termed helix-1) [Ward, E. S., Ellar, D. J., & Chilcott, C. N. (1988) *J. Mol. Biol. 202,* 527–535] of the toxin. Circular dichroism spectroscopy revealed that both segments adopt high α-helical content in a hydrophobic environment, in agreement with previous models. To monitor peptide–lipid and peptide–peptide interactions, the peptides were labeled selectively with either 7-nitro-2,1,3-benzoxadiazol-4-yl (NBD) (to serve as donor) or tetramethylrhodamine (to serve as an acceptor), at their N-terminal amino acids. Both segments bind strongly to small unilamellar vesicles, composed of zwitterionic phospholipids, with surface partition coefficients on the order of 10^4 M^{-1}. The shape of the binding isotherms indicates that helix-2 forms large aggregates within phospholipid membranes. Resonance energy transfer experiments demonstrated that the segments self-associate and interact with each other, but do not associate with unrelated membrane-bound peptides. Functional characterization demonstrated that helix-2 permeates phospholipid SUV with a potency similar to that of naturally occurring pore-forming peptides. Thus, the results support a role for helices-1 and -2 in the assembly and in the pore formation by Bti toxin.

The Gram-positive, spore-forming bacteria *Bacillus thuringiensis* var. *israelensis* (Bti)[1] produce crystalline inclusions that are highly toxic to the larvae of mosquitoes and blackflys (Goldberg & Margalit, 1977). These inclusions contain several polypeptides that are larvicidal and that are cytotoxic for a wide range of cells (Thomas & Ellar, 1983). A 27-kDa toxic protein (Bti toxin) and its corresponding gene have been purified and cloned from Bti isolates (Waalwijk et al., 1985; Ward & Ellar, 1986). Another closely related gene, which differs by only one base pair substitution, was cloned from *B. thuringiensis* var. *morrisoni* (Earp & Ellar, 1987). These 27-kDa proteins are not sequence-homologous to the Cry family of *B. thuringiensis* δ-endotoxins, and therefore have been classified as a unique group of δ-endotoxins, the Cyt (an abbreviation of cytolytic) group (Höfte & Whiteley, 1989). The activated 27-kDa Bti protein is highly cytolytic *in vitro* to a wide range of insects and mammalian cells (Thomas & Ellar, 1983). Furthermore, experiments with lipid dispersions and multilamellar liposomes showed that the toxin bound preferentially to either zwitterionic or positively charged phospholipids (Thomas & Ellar, 1983). Therefore, it is assumed that the interaction between the activated Bti toxin and cell membranes is a protein–lipid interaction, without the assistance of receptors, as is the case with the Cry δ-endotoxins (Gill et al., 1992). It is hypothesized that the Bti toxin exerts its activity via pore formation, ultimately leading to the colloid osmotic lysis of the cells (Thomas & Ellar, 1983; Gill et al., 1987). This is supported by the observation that the toxin can interact with and permeate phospholipid vesicles (Thomas & Ellar, 1983; Drobniewski et al., 1987) as well as form cation-selective single channels in planar lipid membranes (Knowles et al., 1989). Studies on the kinetics of the cellular disruption function of insect Malpighian tubules suggest that the toxic effect occurs as the result of aggregation of several toxin molecules, which are assumed to form a pore (Maddrell et al., 1989). The ion channel activity and the pore formation of the protein might be explained by a model in which transmembrane amphiphilic α-helices form bundles in which their hydrophobic surfaces interact either with other hydrophobic transmembrane segments or with the lipid core of the membrane, and their hydrophilic surfaces point inward, producing a pore (Inouye, 1974; Greenblatt et al., 1985; Guy & Seetrhamulu, 1986; Lear et al., 1988). Indeed, a hydrophobicity plot of the amino acid sequence of Bti revealed the existence of several hydrophobic regions (Ward & Ellar, 1986). Helical wheel analysis (Schiffer & Edmunson, 1967) indicated the existence of a putative amphiphilic α-helical region [amino acids 110–131, designated helix-2 (Ward & Ellar, 1986)] within the major hydrophobic region of the Bti toxin (Ward et al., 1988). In an extensive, site-directed, mutagenesis study, only a mutation within this amphiphilic segment increased the toxicity of the protein *in vitro* (Ward et al., 1988).

Herein, we describe the synthesis, fluorescent labeling, and spectroscopic and functional characterization of two Bti toxin

† This research was supported in part by the Israel Cancer Association, and by the Joseph Cohn Center for Biomembrane Research at the Weizmann Institute of Science, Y.S. is an Incumbent of the Adolpho and Evelyn Blum Career Development Chair in Cancer Research.

* To whom correspondence should be addressed. Telephone: 972-8-342711. Fax: 972-8-344112.

® Abstract published in *Advance ACS Abstracts,* October 15, 1993.

[1] Abbreviations: Boc, butyloxycarbonyl; Bti, *Bacillus thuringiensis* var. *israelensis*; CD, circular dichroism; DCC, dicyclohexylcarbodiimide; DIEA, diisopropylethylamine; HEPES, *N*-(2-hydroxyethyl)piperazine-*N'*-2-ethanesulfonic acid; HOBT, 1-hydroxybenzotriazole; HF, hydrogen fluoride; NBD-F, 4-fluoro-7-nitro-2,1,3-benzoxadiazole; Pam, (phenylacetamido)methyl; PC, egg phosphatidylcholine; PS, phosphatidylserine; RET, resonance energy transfer; RP-HPLC, reverse-phase high-performance liquid chromatography; SUV, small unilamellar vesicle(s); TFA, trifluoroacetic acid; TFE, trifluoroethanol.

0006-2960/93/0432-12363$04.00/0

segments: one with a sequence identical to helix-2 (amino acids 110–131) and the other with a sequence corresponding to helix-1 (amino acids 50–71) (Ward et al., 1988). Circular dichroism (CD) spectroscopy revealed that both peptides adopt highly α-helical structures in a hydrophobic environment. Functional characterization demonstrated that both segments bind strongly to zwitterionic phospholipid small unilamellar vesicles (SUV) and permeate them, with helix-2 being more active than helix-1. Resonance energy transfer measurements, between membrane-bound donor/acceptor-labeled pairs of peptides, demonstrated that the peptides self-associate and interact with each other, but do not associate with unrelated, membrane-bound peptides. Thus, our results are consistent with the proposed role of hydrophobic segments of Bti toxin in its toxic activity (Ward et al., 1986), and assign a possible role for the two hydrophobic segments in the assembly of several Bti toxin molecules to form a pore (Maddrell et al., 1989).

EXPERIMENTAL PROCEDURES

Materials. *t*-Boc-Leu-Pam and *t*-Boc-Thr(Bzl)-Pam resins and dimethylformamide (peptide synthesis grade) were purchased from Applied Biosystems (Foster City, CA), and Boc amino acids were obtained from Peninsula Laboratories (Belmont, CA). Other reagents for peptide synthesis included trifluoroacetic acid (TFA) (Sigma), *N,N*-diisopropylethylamine (DIEA) (Aldrich, distilled over ninhydrin), dicyclohexylcarbodiimide (DCC) (Fluka), and 1-hydroxybenzotriazole (HOBT) (Pierce). Egg phosphatidylcholine (PC) was purchased from Lipid Products (South Nutfield, U.K.). Cholesterol (extra pure) was supplied by Merck (Darmstadt, Germany) and recrystallized twice from ethanol. 5- and 6-carboxytetramethylrhodamine succinimidyl ester and 3,3′-diethylthiodicarbocyanine iodide (diS-C_2-5) were obtained from Molecular Probes (Eugene, OR). NBD-F (4-fluoro-7-nitro-2,1,3-benzoxadiazole) was obtained from Sigma. All other reagents were of analytical grade. Buffers were prepared in double glass-distilled water.

Peptide Synthesis and Purification. The peptides were synthesized by a solid phase method on *t*-Boc-Leu or *t*-Boc-Thr(Bzl) Pam resins (0.05 mequiv) (Merrifield et al., 1982). The peptides were cleaved from the resins by HF and extracted with dry ether after HF evaporation. The crude peptides contained one major peak (as revealed by RP-HPLC), which was shown to be >90% pure peptide by weight. The peptides were then purified by RP-HPLC on a cyano (CN) reverse-phase column (4 mm/250 mm, DuPont). The column was eluted in 40 min, at a flow rate of 0.6 mL/min, using a linear gradient of 25–80% acetonitrile in water in the presence of 0.1% TFA (v/v). The purified peptides were shown to be homogeneous (~99%) by analytical HPLC, and their compositions were confirmed by amino acid analysis.

Fluorescent Labeling of Peptides. Labeling of the N-terminus of the peptides with fluorescent probes was achieved as previously described (Rapaport & Shai, 1992). Briefly, 10 mg of resin-bound peptides (3–4 μmol) was treated with TFA (50% v/v in methylene chloride) in order to remove the Boc protecting group from the N-terminal amino groups of the linked peptides. The resin-bound peptides were then reacted with either (i) tetramethylrhodamine succinimidyl ester (Rhosuc) (3–4 equiv) in dry dimethylformamide containing 5% v/v diisopropylethylamine or (ii) NBD-F in dimethylformamide. The peptides were then cleaved from the resins by HF, and finally precipitated with ether. All peptides were purified using RP-HPLC as described in the previous section.

Preparation of Liposomes. Small unilamellar vesicles (SUV) were prepared by sonication of PC. Briefly, dry lipid and cholesterol (10:1 w/w) were dissolved in a $CHCl_3$/MeOH mixture (2:1 v/v). The solvents were then evaporated under a stream of nitrogen, and the lipids were put under vacuum for 1 h and then resuspended in the appropriate buffer (at a concentration of 7.2 mg/mL), via vortex mixing. The resultant lipid dispersion was then sonicated for 5–15 min in a bath-type sonicator (G1125SP1 sonicator; Laboratory Supplies Company Inc., New York, NY) until clear. The lipid concentration of the supernatant was determined by phosphorus analysis (Bartlett et al., 1959). Vesicles were visualized by using a JEOL JEM 100B (Japan Electron Optics Laboratory Co., Tokyo, Japan) electron microscope as follows: A drop of vesicles was deposited on a carbon-coated grid and negatively stained with uranyl acetate. The grids were examined, and the vesicles were shown to be unilamellar with an average diameter of 20–50 nm (Papahadjopoulos & Miller, 1967).

CD Spectroscopy. The CD spectra of the peptides were measured with a Jasco J-500A spectropolarimeter. The spectra were scanned in a capped quartz optical cell with 0.5-mm path length, at 25 °C. Spectra were obtained at wavelengths from 250 to 190–200 nm. A total of 8–12 scans were taken at a scan rate of 20 nm/min. The peptides were scanned at concentrations of 2.0×10^{-5} M, in methanol, buffer (50 mM Na_2SO_4/25 mM HEPES–sulfate, pH 6.8), and in the presence of SUV composed of zwitterionic phospholipids. Fractional helicities (Wu et al., 1981) were calculated as

$$f_h = \frac{[\theta]_{222} - [\theta]^0_{222}}{[\theta]^{100}_{222}}$$

where $[\theta]_{222}$ is the experimentally observed mean residue ellipticity at 222 nm and values for $[\theta]^0_{222}$ and $[\theta]^{100}_{222}$, corresponding to 0% and 100% helix content at 222 nm, were estimated at 2000 and 30 000 deg·cm^2/dmol, respectively (Chen et al., 1974; Wu et al., 1981).

Spectrofluorometric Studies. (*A*) *NBD Fluorescence Measurements.* NBD-labeled peptides (0.2 nmol) were added to 2 mL of buffer (50 mM Na_2SO_4/25 mM HEPES–sulfate, pH 6.8) containing 815 μg of PC–SUV to establish a lipid:peptide ratio (4000:1) at which all the peptides are bound to lipids. After a 2-min incubation, the emission spectrum of the NBD group was recorded (in three separate experiments) using a Perkin-Elmer LS-50B spectrofluorometer, with excitation set at 467 nm (10-nm slit).

(*B*) *Binding Experiments.* Binding experiments were conducted as previously described (Rapaport & Shai, 1991). Briefly, PC SUV were added successively to a 0.1 μM sample of labeled peptide at 25 °C. Fluorescence intensity was measured as a function of the lipid:peptide molar ratio on a Perkin-Elmer LS-50B spectrofluorometer, with excitation set at 467 nm, using a 10-nm slit, and emission set at 530 nm, using a 5-nm slit, in three separate experiments. In order to account for the background signal contributed by the lipids to any given signal, the readings observed when unlabeled peptides were titrated with lipid vesicles were subtracted from each recording of fluorescence intensity.

The binding isotherms were analyzed as a partition equilibrium (Schwarz et al., 1987; Rizzo et al., 1987; Beschiaschvili & Seelig, 1990; Rapaport & Shai, 1991), using the equation:

$$X_b = K_p C_f$$

where X_b is defined as the molar ratio of bound peptide (C_b)

per total lipid (C_L), K_p corresponds to the partition coefficient, and C_f represents the equilibrium concentration of free peptide in the solution. To calculate X_b, f_b (the fraction of membrane-bound peptide) was calculated using the equation:

$$f_b = (F - F_0)/(F_\infty - F_0)$$

in which F_∞ (the fluorescence signal obtained when all the peptide is bound to lipid) was extrapolated from a double-reciprocal plot of F (total peptide fluorescence) versus C_L (total concentration of lipids) (Schwarz et al., 1987), F_0 is the fluorescence intensity of unbound peptide, and F is the fluorescent intensity of bound peptide.

Having calculated the value of f_b, it was possible to calculate C_f, as well as the extent of peptide binding, X_b. In practice, it was assumed that the peptides were initially partitioned only over the outer leaflet of the SUV (60% of the total lipid), as had been previously suggested (Beschiaschvili & Seelig, 1990). Therefore, values of X_b were corrected as such:

$$X_b^* = X_b/0.6$$

and the partition equation became

$$X_b^* = K_p^* C_f$$

The curve resulting from plotting X_b^* versus free peptide, C_f, is referred to as the conventional binding isotherm.

Resonance Energy Transfer Measurements and Calculations. Fluorescence spectra were obtained at room temperature in a Perkin-Elmer LS-50B spectrofluorometer, with the excitation monochromator set at 467 nm (to minimize the excitation of tetramethylrhodamine) with a 5-nm slit width. Measurements were performed in a 1-cm path-length, quartz cuvette in a final reaction volume of 2 mL. In a typical experiment, donor peptide (final concentration 0.02 μM) was added to a dispersion of PC SUV in buffer (50 mM Na_2SO_4/25 mM HEPES–sulfate, pH 6.8), followed by the addition of acceptor peptide in several sequential doses. Fluorescence spectra were obtained before and after addition of the acceptor. Any changes in the fluorescence intensity of the donor, due to processes other than energy transfer to the acceptor, were determined by substituting unlabeled peptide in place of the acceptor, and by measuring the emission spectrum of the acceptor alone in the presence of vesicles.

The efficiency of energy transfer (E) was determined by measuring the decrease in the quantum yield of the donor as a result of the addition of acceptor. E was determined experimentally from the ratio of the fluorescence intensities of the donor in the presence (I_{da}) and in the absence (I_d) of the acceptor at the donor's emission wavelength, after correcting for membrane light scattering and the contribution of the acceptor's emission. The percentage of transfer efficiency (E) is defined as

$$E = (1 - I_{da}/I_d)100$$

The correction for light scattering was made by subtracting the signal obtained when unlabeled analogues were added to vesicles containing the donor molecule. Correction for the contribution of acceptor emission was made by subtracting the signal produced by the acceptor-labeled analogue alone.

The distance (in angstroms) between the donor and acceptor at which the transfer efficiency is 50% (R_0) was calculated by the equation:

$$R_0 = (J\kappa^2 Q_D n^{-4})^{1/6}(9.79 \times 10^3)$$

where J is determined from the integral of the spectral overlap of the donor emission and the acceptor absorption, κ^2 is the dipole–dipole orientation factor, Q_D is the quantum yield of the donor in the absence of acceptor, and n is the refractive index of the medium (Förster, 1959). In our calculations, the refractive index of the medium is 1.5 (Fung & Strier, 1978), the NBD quantum yield was taken to be 0.75 (Connor & Schroit, 1987), and the orientation factor is taken to be $^2/_3$, assuming random orientation between donor and acceptor dipoles.

Fluorometric Detection of Membrane Pores. Pore-mediated diffusion potential assays (Sims et al., 1974; Loew et al., 1983) were performed as previously described (Shai et al., 1990, 1991). In a typical experiment, 4 μL (28.8 μg) of a liposome suspension, prepared in K^+ buffer (50 mM K_2SO_4/25 mM HEPES–sulfate, pH 6.8), was diluted in 1 mL of isotonic K^+-free buffer (50 mM Na_2SO_4/25 mM HEPES–sulfate, pH 6.8) in a glass tube, to which the fluorescent, potential-sensitive dye diS-C_2-5 was then added. A 1-μL sample of a 10^{-7} M valinomycin solution was then added to the suspension in order to slowly create a negative diffusion potential inside the vesicles, which lead to a quenching of the dye's fluorescence. Once the fluorescence had stabilized, 3–10 min later, peptides were added. The subsequent dissipation of the diffusion potential, which was reflected as an increase in fluorescence, was monitored on a Perkin Elmer LS-50B spectrofluorometer, with excitation set at 620 nm and emission at 670 nm, with the gain adjusted to 100%. The percentage of fluorescence recovery, F_t, was defined as

$$F_t = [(I_t - I_0)(I_f - I_0)]100$$

where I_0 = the initial fluorescence, I_f = the total fluorescence observed before the addition of valinomycin, and I_t = the fluorescence observed after adding the peptide, at time t.

RESULTS

To evaluate a functional role for specific segments of the Bti toxin in its toxic activity, two 22 amino acid containing peptides were synthesized by a solid phase method: one with a sequence identical to the putative amphiphilic α-helix region of the Bti 27-kDa cytolytic toxin (designated helix-2, and comprised of amino acids 110–131), and the other with a sequence corresponding to helix-1 of the protein (amino acids 50–71). Each peptide was labeled selectively at its N-terminal amino acid either with the environmentally sensitive NBD (to serve as a donor) or with tetramethylrhodamine (Rho, to serve as an energy acceptor). Table I shows the sequences of the Bti peptides, their fluorescent derivatives, and their designations, including those of control membrane-permeating peptides. The peptides were characterized by a variety of biophysical methods in order to determine the following: (i) their secondary structure in methanol, in solution, or in the presence of phospholipid membranes; (ii) their binding properties to zwitterionic phospholipid membranes; (iii) their ability to self-associate and to form heteroaggregates in their membrane-bound states; (iv) their ability to permeate phospholipid SUV.

CD Spectroscopy. The extent of the α-helical secondary structure of helix-2 and helix-1 was estimated from their CD spectra (Wu et al., 1981) in three solutions: in a hydrophobic environment (methanol), in aqueous buffer, and in buffer containing SUV composed of zwitterionic phospholipids (Figure 1). Helix-2 exhibited mean residual ellipticities, $[\theta]_{222}$, of 18 770, 12 360, and 15 330 deg·cm^2/dmol, in methanol, in buffer, and in the presence of phospholipids, respectively. These values correspond to relatively high α-helicities of 55.9%, 34.5%, and 44.4% in the three solvent systems, respectively.

Table I: Amino Acid Sequences of Bti and Its Fluorescent-Labeled Segments, and of the Control Peptides

peptide no.	peptide designation	sequence
1	helix-2	HN_2-NQVSVMINKVLEVLKTVLGVAL-COOH
2	NBD-helix-2	**NBD**-NQVSVMINKVLEVLKTVLGVAL-COOH
3	Rho-helix-2	**Rho**-NQVSVMINKVLEVLKTVLGVAL-COOH
4	helix-1	HN_2-NYILQAIMLANAFQNALVPTST-COOH
5	NBD-helix-1	**NBD**-NYILQAIMLANAFQNALVPTST-COOH
6	Rho-helix-1	**Rho**-NYILQAIMLANAFQNALVPTST-COOH
7	Rho-Na-S-4[a]	**Rho**-RTFRVLRALKTITIFPGLKTIVRA-COOH
8	Rho-pardaxin[b]	**Rho**-GFFALIPKIISSPLFKTLLSAVGSAL-SSSGGQE-COOH

[a] Taken from Rapaport et al. (1992). [b] Taken from Rapaport and Shai (1991).

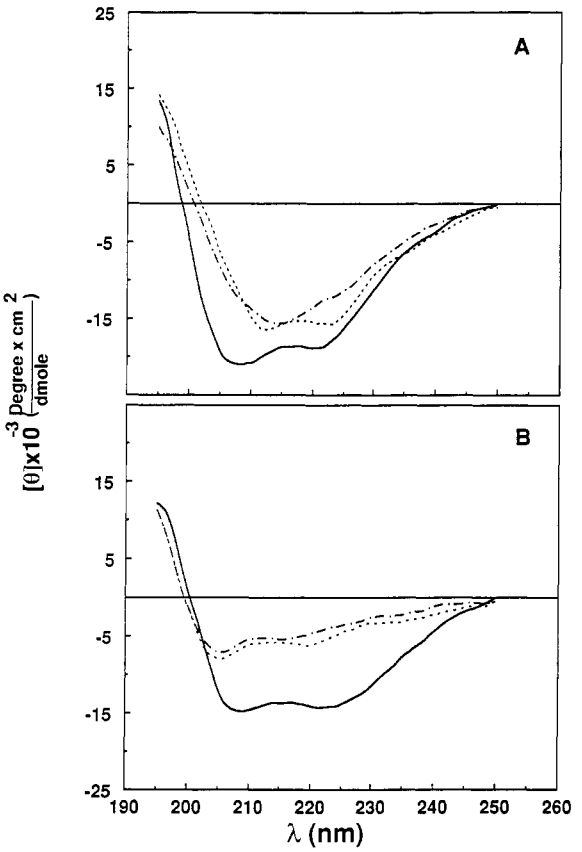

FIGURE 1: CD spectra of helix-1 and helix-2 in different solvents. Spectra were taken as described under Experimental procedures at a peptide concentration of 2.0×10^{-5} M. Panel A, helix-2; panel B, helix-1. Continuous line, in methanol; dashed–dotted line, in buffer; dotted line, in the presence of vesicles.

On the other hand, helix-1 exhibited mean residual ellipticities, $[\theta]_{222}$, of 14 500, 4300, and 5430 deg·cm^2/dmol, corresponding to fractional helicity values of 41.7%, 7.7%, and 11.5% in methanol, in buffer, and in the presence of vesicles, respectively. It should be noted that the CD spectra of helix-2 and helix-1 in the presence of vesicles were obtained at the optimal peptide: lipid molar ratio of 0.038, to avoid interference of light scattering due to high concentrations of vesicles. Under these conditions, the amounts of the peptides bound to the vesicles, as calculated from their binding isotherms (Figures 2 and 3), are 43% and 6% for helix-2 and helix-1, respectively.

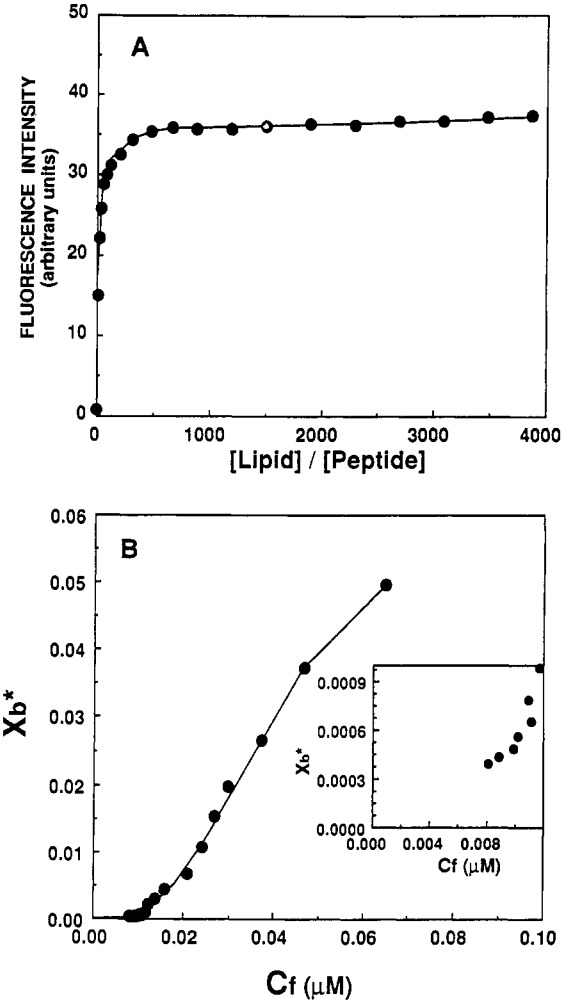

FIGURE 2: (A) Increase in the fluorescence of NBD-helix-2 upon titration with PC vesicles. Peptide (0.1 μM) was titrated with PC vesicles with excitation monitored at 467 nm and emission recorded at 530 nm. The experiment was performed at 24 °C in 50 mM Na_2SO_4/25 mM HEPES–sulfate, pH 6.8. (B) Binding isotherm derived from panel A by plotting X_b* (molar ratio of bound peptide per 60% lipid) versus C_f (equilibrium concentration of free peptide in the solution). The inset shows the low concentration range of the main figure.

Therefore, the marked difference in their CD spectra, in the presence of vesicles, might reflect different levels of the fractions bound.

Fluorescence Studies. (A) Location of the NBD Moiety in Hydrophobic Environments. The environmentally sensitive NBD fluorophore has been utilized previously in polarity and binding studies (Kenner & Aboderin, 1971; Frey & Tamm, 1990; Rapaport & Shai, 1991). Herein, the intrinsic fluorescence of NBD-helix-1, NBD-helix-2, and NBD-aminoethanol (a control) was monitored in aqueous solutions or in the presence of zwitterionic PC SUV vesicles. SUV were used to minimize differential light-scattering effects (Mao & Wallace, 1984), and zwitterionic vesicles were used to avoid contributions of phospholipid head-group charges to binding processes. In these experiments, the lipid:peptide molar ratios were elevated (4000:1) so that spectral contributions of free peptides would be negligible. Both NBD-helix-1 and NBD-helix-2 exhibited fluorescence emission maxima at 547 ± 1 nm in buffer, which reflect hydrophilic environments for the NBD moieties (Kenner & Aboderin, 1971; Rajarathnam et al., 1989; Rapaport & Shai, 1991). However, upon addition of PC vesicles to aqueous solutions containing NBD-labeled peptides, a blue shift in the emission maxima (toward 525–

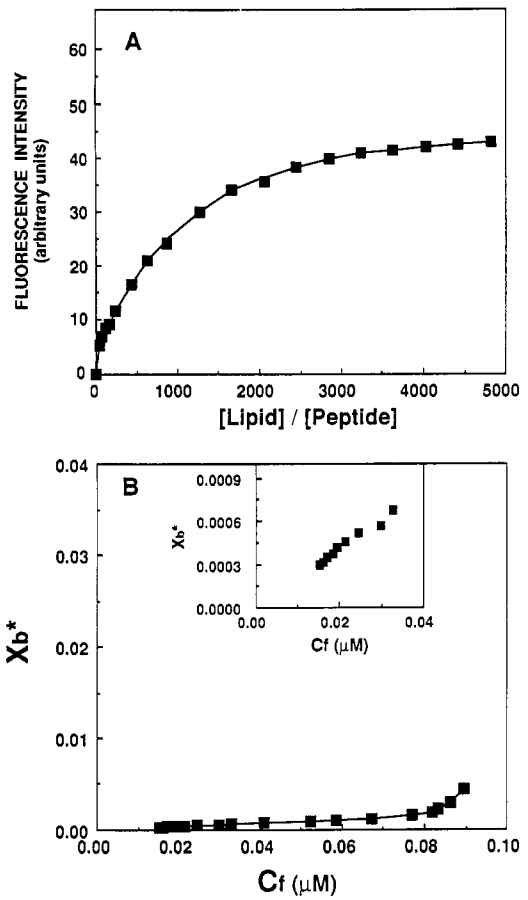

FIGURE 3: (A) Increase in the fluorescence of NBD-helix-1 upon titration with PC vesicles. (A) Peptide (0.1 μM) was titrated with PC vesicles with excitation monitored at 467 nm and emission recorded at 530 nm. The experiment was performed at 24 °C in 50 mM Na_2SO_4/25 mM HEPES–sulfate, pH 6.8. (B) Binding isotherm derived from panel A by plotting X_b* (molar ratio of bound peptide per 60% lipid) versus C_f (equilibrium concentration of free peptide in the solution). The inset shows the low concentration range of the main figure.

526 nm, data not shown) and a marked increase in the fluorescence intensities of the NBD groups were observed. Both these changes reflect relocation of the NBD groups into the hydrophobic environment of the lipid bilayer (Chattopadhyay & London, 1987; Frey & Tamm, 1990; Rapaport & Shai, 1991). No shift in the emission maximum was detected when the control, NBD-aminoethanol, was used under the same conditions.

(B) Characterization of Binding Isotherms and Determination of Partition Coefficients. The fluorescent increase of the NBD-labeled peptides, in the presence of PC vesicles, enabled the generation of binding isotherms, from which partition coefficients could be calculated as previously described (Frey & Tamm, 1990; Rapaport & Shai, 1991). The increases in the fluorescence intensities of the NBD-labeled peptides (0.1 μM), as a function of lipid:peptide molar ratios, were plotted and yielded conventional binding curves (Figures 2A and 3A, for NBD-helix-2 and NBD-helix 1, respectively). When unlabeled helix-2 or helix-1 was titrated with lipids, up to the maximal concentration used with the NBD-labeled peptides, the fluorescence intensities of these solutions, after subtracting the contribution of the vesicles, remained unchanged.

The binding curves were analyzed as partition equilibria, as described under Experimental Procedures. The resulting binding isotherms were obtained by plotting X_b* (the molar ratio of bound peptide per 60% of total lipid) versus C_f (the equilibrium concentration of free peptide in solution). The experimental binding isotherms of the interactions of NBD-helix-2 and NBD-helix-1 with PC SUV are given in Figures 2B and 3B, respectively. The surface partition coefficients were estimated by extrapolating the initial slopes of the curves to zero C_f values. The estimated surface partition coefficient, K_p*, of NBD-helix-2 is 5.1 × 10^4 M^{-1}, and that of NBD-helix-1 is 2.1 × 10^4 M^{-1}. These K_p* values are within the range of those obtained for membrane-permeating bioactive peptides, such as melittin and its derivatives (Stankowski & Schwarz, 1990), *Staphylococcus* δ-toxin (Thiaudière et al., 1991), the antibiotic dermaseptin (Pouny et al., 1992), and pardaxin and its analogues (Rapaport & Shai, 1991).

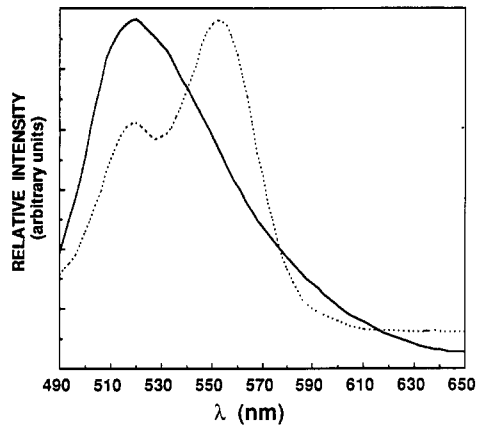

FIGURE 4: Spectral overlap between the absorption spectrum of Rho-helix-2 (0.05 μM) (continuous line) and the fluorescence emission spectrum of NBD-helix-2 (0.05 μM) (dotted line) at an excitation wavelength of 467 nm in phospholipid vesicles composed of egg PC at a lipid:peptide molar ratio of 1400:1.

The shapes of the binding isotherms of peptides have been proposed to provide information about the organization of peptides within membranes (Schwarz et al., 1987). The shapes of the binding isotherms of NBD-helix-2 and NBD-helix-1 are different. The binding isotherm of NBD-helix-2 displays an initial "lag"; i.e., the curve is initially flat but eventually rises sharply upon crossing the threshold concentration (corresponding to low C_f values). On the other hand, the isotherm obtained with NBD-helix-1 is practically flat, but rises only slightly at high C_f values. The shape of the NBD-helix-2 isotherm argues in favor of a process whereby peptides first incorporate into the membrane and then once inside the membrane aggregate to form a pore (Schwarz et al., 1987; Rapaport & Shai, 1991). Similar behavior was observed with alamethicin, although at much higher C_f values (Rizzo et al., 1987), pardaxin and some of its derivatives that are postulated to form aggregation-derived pores in lipid bilayers (Rapaport & Shai, 1991), the S-4 segment of the sodium channel in acidic vesicles (Rapaport et al., 1992), and the α5 segment of *Bacillus thuringiensis* δ-endotoxin (Gazit & Shai, 1993). The binding isotherm of NBD-helix-1 suggests that an aggregational state of the segments may occur within the membrane only at high peptide:lipid molar ratios.

Resonance Energy Transfer (RET) Experiments. (A) Suitability of the NBD/Rho Pair for Studies of RET between Peptide Molecules. The emission spectrum of NBD-helix-2 (the donor) and the absorption spectrum of Rho-helix-2 (the acceptor) are given in Figure 4. On the basis of the spectral overlap of the NBD-helix-2 emission, and the Rho-helix-2 absorption spectra presented in Figure 4, the R_0 value for the NBD-helix-2/Rho-helix-2 donor/acceptor pair was calculated to be 51.1 Å.

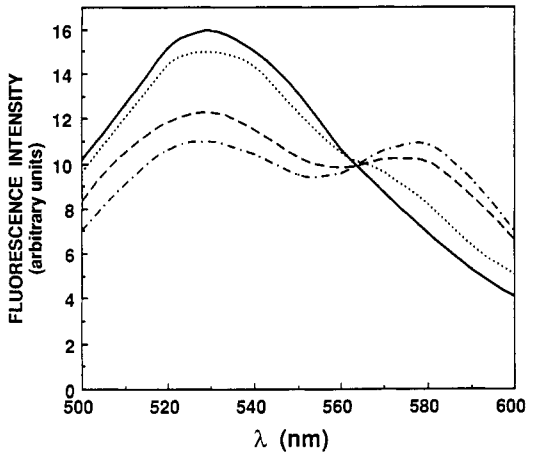

FIGURE 5: Fluorescence energy transfer dependence on Rho-peptide (acceptors) concentrations using PC vesicles. The spectrum of NBD-helix-2 (0.02 μM), the donor peptide, was determined in the presence or absence of various concentrations of the acceptor peptide, Rho-helix-2. Each spectrum was recorded in the presence of PC vesicles (100 μM) in 50 mM Na_2SO_4/25 mM HEPES–sulfate, pH 6.8. The excitation wavelength was set at 467 nm; emission was scanned from 500 to 600 nm. The spectra of Rho-helix-2, in the presence of vesicles and unlabeled helix-2, were subtracted from the corresponding spectra. (—) 0.02 μM NBD-helix-2; (···) mixture of 0.02 μM NBD-helix-2 and 0.01 μM Rho–helix-2; (– –) mixture of 0.02 μM NBD-helix-2 and 0.02 μM Rho-helix-2; (– · –) mixture of 0.02 μM NBD-helix-2 and 0.04 μM Rho-helix-2.

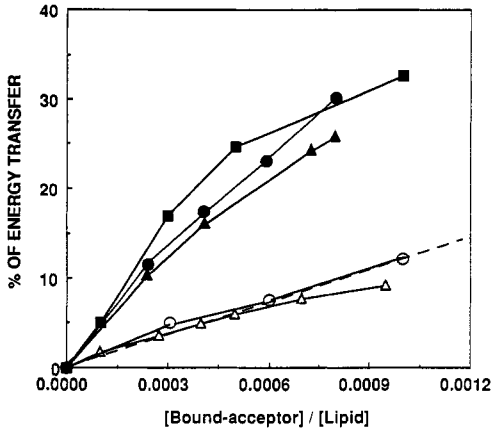

FIGURE 6: Theoretically and experimentally derived percentage of energy transfer versus bound acceptor:lipid molar ratio. The amount of lipid-bound acceptor (Rho-peptides), C_b, at various acceptor concentrations was calculated as described under Results. Filled circles, NBD-helix-1/Rho-helix-1; filled squares, NBD-helix-2/Rho-helix-2; filled triangles, NBD-helix-2/Rho-helix-1; open circles, NBD-helix-2/Rho-Na-S-4; open triangles, NBD-helix-2/Rho-pardaxin (NBD-helix-1/Rho-Na-S-4 or NBD-helix-1/Rho-pardaxin pairs gave similar results and therefore were omitted to prevent clustering); dashed line, random distribution of the monomers (Fung & Stryer, 1978), assuming an R_0 of 51.1 Å.

In the RET experiments, either NBD-helix-2 or NBD-helix-1 served as donor. Examples of profiles of the energy transfer from NBD-helix-2 to Rho-helix 2, in the presence of PC phospholipid vesicles, are depicted in Figure 5. Addition of Rho-helix-2, Rho-helix-1, Rho-pardaxin, or Rho-Na-S-4 (final concentrations of 0.01–0.1 μM) to NBD-helix-2 (0.02 μM) in the presence of PC phospholipid vesicles (100 μM) quenched the donor's emission and increased the acceptor's emission, which is consistent with energy transfer. These emission changes were marked with Rho-helix-2 and Rho-helix-1, but not with the other Rho-labeled peptides. Similar experiments were performed with NBD–helix-1 as a donor and Rho-helix-1, Rho-pardaxin, or Rho-Na-S-4 (final concentrations of 0.01–0.1 μM) as acceptors. In control experiments, no change in the emission spectrum of NBD was observed when the Rho-labeled peptides were replaced by equal amounts of unlabeled peptides (data not shown). To determine the actual percentage of energy transfer, the amounts of lipid-bound acceptors, C_b (Rho-peptides, termed "bound-acceptor"), at various Rho-peptide concentrations were calculated from the binding isotherms of the corresponding NBD-labeled peptides as follows. First, the fractions of bound acceptor, f_b, were calculated for the various peptide:lipid molar ratios depicted and in Figures 2A and 3A, or from the binding isotherms given in Rapaport and Shai (1991) and Rapaport et al. (1992). Having calculated these values of f_b, it is then possible to calculate the fraction bound, C_b ($C_b = 0.1 f_b$). The curves of the experimentally-derived percentage of energy transfer versus the bound-acceptor:lipid molar ratios are depicted in Figure 6. A curve corresponding to a random distribution of monomers, assuming an R_0 of 51.1 Å as calculated for the NBD/Rho donor/acceptor pair and assuming that the surface density of donors (donor/lipid) is 0.01 (Fung & Stryer, 1978), is also depicted. A high percentage of energy transfer was obtained with NBD-helix-2/Rho-helix-2, NBD-helix-1/Rho-helix-1, and NBD-helix-2/Rho-helix-1 pairs (Figure 6). These values are markedly higher than those obtained assuming a random distribution of monomers. High energy transfer between the NBD-helix-1/Rho-helix-1 or NBD-helix-2/Rho-helix-1 pairs required higher total peptide:lipid molar ratios than with the NBD-helix-2/Rho-helix-2 pair (Figure 4). For example, 2-fold higher peptide:lipid molar ratios were required to reach 25% energy transfer. Efficiencies of energy transfer between NBD-helix-2 and the unrelated membrane-interacting peptides, Rho-pardaxin and Rho-Na-S-4, resemble those observed for random distribution. Therefore, these unrelated peptides do not appear to interact with NBD-helix-2. Thus, it can be concluded that the donor NBD-helix-2 and the acceptor Rho-helix-2 and Rho-helix-1 and that the donor NBD-helix-1 and the acceptor Rho-helix-1 are specifically associated, rather than randomly distributed throughout the membrane.

(*B*) *Valinomycin-Mediated Diffusion Potential Assay.* To examine the efficacy of Bti peptides to perturb the lipid packing of membranes and to cause leakage of vesicular contents, the peptides' ability to dissipate a diffusion potential of SUV was examined. Increasing concentrations of the helix-2 or helix-1 segments or of their fluorescently-labeled analogues were mixed with SUV composed of PC that had been pretreated with the fluorescent, potential-sensitive dye diS-C_2-5 and valinomycin. Recovery of fluorescence was monitored with time, with peptide:lipid molar ratios of 0.009:1 to 0.9:1. The maximal potential of the peptides to permeate the membranes was elucidated by monitoring the fluorescence recovery until a plateau was observed, usually 10–30 min (Figure 7). The inset shows typical profiles of fluorescence recovery as a function of time for helix-2 and helix-1, using PC vesicles, at the indicated lipid:peptide molar ratios. Similar profiles were obtained using fluorescently-labeled helix-2 or helix-1 analogues. The results demonstrate that helix-2 has a higher membrane-permeating activity compared to helix-1.

DISCUSSION

Bti toxin interacts with and permeates cell membranes (Gill et al., 1992; Hofte & Whiteley, 1989). These properties are characteristic of naturally-occurring, membrane-permeating, short polypeptides (26–35 amino acids long), such as the bee venom melittin, the shark repellent neurotoxin pardaxin, and

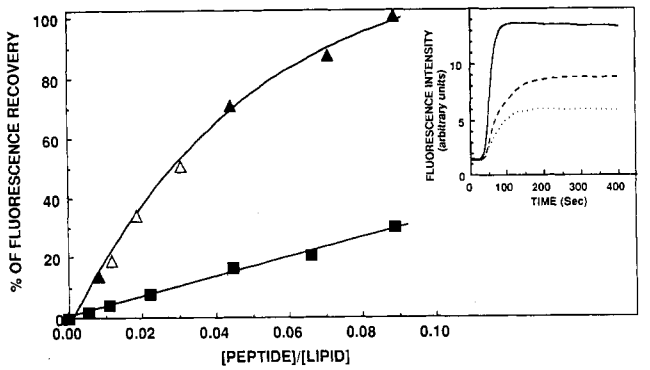

FIGURE 7: Maximal dissipation of the diffusion potential in vesicles induced by helix-1 and helix-2. The peptides were added to isotonic K^+-free buffer containing SUV composed of zwitterionic phospholipids, preequilibrated with the fluorescent dye diS-C_2-5 and valinomycin. Fluorescence recovery, measured 10 min after mixing the peptides with the vesicles, is depicted. Filled triangles, helix-2; filled squares, helix-1; open triangles, NBD-helix-2. Inset: Typical profiles of the kinetics of dissipation of the diffusion potential in vesicles. Peptide designation and peptide:lipid molar ratios are as follows: continuous line, helix-2, 3.38 μM; dashed line, helix-2, 1.69 μM; dotted line, helix-1, 3.38 μM.

the antimicrobial peptides magainin, cecropin, and dermaseptin. Some of these toxins are believed to exert their permeating activity via pore formation, as is also hypothesized for Bti toxin (Ward et al., 1988; Thomas & Ellar, 1983). A common structural feature of this family of toxins is their potential to form amphiphilic α-helix structures, as envisioned from their wheel projections (Schiffer & Edmunson, 1967). The amphiphilic α-helical structure is considered to be an essential secondary structure motif required for pore formation. According to proposed models, pores are formed via the aggregation of transmembrane, amphiphilic α-helices, such that their hydrophobic surfaces interact either with other hydrophobic transmembrane segments or with the lipid constituents of the membrane, and their hydrophilic surfaces point inward, producing a pore (Inouye, 1974; Greenblatt et al., 1985; Guy & Seetrhamulu 1986; Lear et al., 1988). Indeed, a hydrophobicity plot of the amino acid sequence of Bti toxin revealed putative hydrophobic segments. Only one of them (helix-2) has the potential to form an amphiphilic α-helical structure, and only a mutation within this amphiphilic segment increased the toxicity of the Bti toxin *in vitro* (Ward & Ellar, 1986; Ward et al., 1988). Kinetic measurements suggest that the aggregation of several molecules of Bti toxin causes the cellular disruption function of insect malpighian tubules (Maddrell et al., 1989). This is in line with the hypothesis that the Bti toxin pore is formed by a bundle of α-helices from several toxin molecules.

We investigated the possible involvement of helix-2 (amino acids 110–131) and of helix-1 (amino acids 50–71) in the toxicity mechanism of Bti toxin by examining their structure–function relationship utilizing a spectrofluorometric approach. Zwitterionic PC phospholipids were used as a model system to prevent the contribution of the phospholipid head-group charges to the binding processes, and also since they preferentially bind the entire Bti toxin (Thomas & Ellar, 1983). When limited binding and membrane-permeating experiments were performed with the negatively charged PS/PC vesicles, similar results to those with PC vesicles were obtained (data not shown).

Secondary structure determination, using CD spectroscopy, revealed that both segments adopt high α-helix structures in a hydrophobic environment (Figure 1), which agrees with a proposed structural model of the toxin (Ward et al., 1988). However, in the presence of phospholipid vesicles, only helix-2 adopts high α-helix structure. This is probably due to the high fraction (43%) of membrane-bound helix-2 as compared to 6% with helix-1, calculated from their binding isotherms. Similarly, highly α-helical contents in hydrophobic environments are present in various naturally-occurring, membrane-permeating polypeptides. Examples are the bee venom melittin (Vogel, 1981), the shark repellent neurotoxin pardaxin (Shai et al., 1990, 1991), bombinin-like peptides (Gibson et al., 1991), and various antimicrobial peptides, such as alamethicin (Rizzo et al., 1987), magainin (Chen et al., 1988), cecropins (Andreu et al., 1985), and dermaseptin (Mor et al., 1991).

Fluorometric studies, based on the environmentally sensitive fluorophore NBD selectively attached to the N-terminus of the Bti helices, allowed determination of three important properties of helix-1 and helix-2. (i) Both bind to zwitterionic phospholipid vesicles with high affinity, comparable to those of naturally-occurring, membrane-permeating peptides, such as melittin and its derivatives (Stankowski & Schwarz, 1990), the *Staphylococcus* δ-toxin (Thiaudière et al., 1991), the antibiotics alamethicin (Rizo et al., 1987) and dermaseptin (Pouny et al., 1992), and the shark repellent neurotoxin pardaxin and its analogues (Rapaport & Shai, 1991; Pouny & Shai, 1992). (ii) The N-termini of both segments locate within the lipidic environment of the vesicles, as demonstrated by the findings that the maximum emission wavelengths (525–526 nm) observed for both NBD-helix-2 and NBD-helix-1 in the presence of vesicles are significantly lower than that (533 nm) observed for a NBD group located in a hydrophilic environment or on the surface of vesicles (Chattopadhyay & London, 1987). (iii) Helix-2 seems to form large aggregates within the membrane at relatively low peptide: lipid molar ratios, while helix-1 does not. This assumption is based on the observation of an upward curvature of the binding isotherm of NBD-helix-2 at low C_f values (Figure 2) and the slight curvature of NBD-helix-1 at higher C_f values (Figure 3). The upper curvature of NBD-helix-2 is similar to those obtained for the channel-forming peptides pardaxin (Rapaport & Shai, 1991) and alamethicin (Rizzo et al., 1987), which argues in favor of a process whereby peptides first incorporate into the membrane and then aggregate.

The self-assembly between fluorescently-labeled helix-1 or helix-2 segments, or a coassembly between them, was implied by RET experiments (Figures 5 and 6). However, other membrane-embedded polypeptides, such as Rho-Na-S-4 (which is randomly distributed in its membrane-bound state; Rapaport et al., 1992) or Rho-pardaxin (which self-aggregates within membranes; Rapaport & Shai, 1992), do not assemble with either helix-1 or helix-2 (Figure 6). This implies that the helix-1 and helix-2 segments can specifically interact with each other, but not with unrelated membrane-bound polypeptides. Due to the low ability of helix-1 to form aggregates at low C_f values (Figure 3), higher concentrations of helix-1 (than of helix-2) were required to detect significant energy transfer. This might imply that the probability of Bti monomers packing correctly to form a pore is governed predominantly by helix-2. Since several Bti toxin monomers are required to form the pore, the effect of the reduced partitioning within the membrane of helix-1 on its probability to assist in the assembly of monomers to form a functional pore is even more pronounced.

The results reported here support accumulating data that intramembranal α-helices of integral membrane proteins can participate in specific interactions that contribute to the specific recognition, association, and oligomerization of those proteins

within the lipid environment (Popot & Engelman, 1990). These interactions are described by a "two stage" model for membranal protein folding and oligomerization (Popot et al., 1987; Popot & Engelman, 1990). In the first stage, independent, thermodynamically-stable α-helices are formed within the lipid bilayers, which leads to the second stage of assembly and oligomerization of the segments within the membranes. This model can explain the formation of an active molecule of bacteriorhodopsin by the assembly of two enzymatically-cleaved, single, transmembrane α-helices, and a third segment composed of five transmembrane α-helices (Kahn & Engelman, 1992). Other examples of such participation of intramembranal sequences of proteins in peptide–peptide interactions are the dimerization of glycophorin A (Bormann et al., 1989; Lemmon et al., 1992), the specific association between transmembrane segments in the aspartate sensory receptor of *Escherichia coli* (Lynch & Koshland, 1991), the dimerization of the T cell receptor complex (Bonifacino et al., 1990; Manolios et al., 1990) and the growth factor receptors (Sternberg & Gullick, 1990), and the self-association of the single transmembrane segment of the minK potassium channel (Ben-Efraim et al., 1993). These examples and others [see review by lemmon and Engelman (1992)] suggest that protein sequences within the membranes can contribute to the specific recognition and assembly of other proteins as well. Accumulating data also suggest that synthetic peptides, corresponding to the transmembrane segments of various ion channels, might be involved in their channel formation (Oiki et al., 1988; Tosteson et al., 1989; Rapaport et al., 1992; Grove et al., 1991; Ghosh & Stroud, 1991; Langosch et al., 1991; Ben-Efraim et al., 1993).

The fact that helix-2 can permeate phospholipid vesicles better than helix-1 (Figure 7) may be due to its higher ability to form aggregates within the membrane, as revealed from their binding isotherms (Figures 2 and 3). Thus, at comparable peptide:lipid molar ratios, more molecules of helix-2 are bound to the vesicles. It should be noted that the whole Bti toxin bound better to zwitterionic phospholipids than to acidic ones (Thomas & Ellar, 1983). Our studies with the synthetic segments did not reveal any significant differences between the binding properties and the permeating potencies of the segments to PC or to acidic PS/PC phospholipids (data not shown). These results might imply (although further studies are required) that other parts of the toxin, which contain acidic amino acids, are exposed on the surface of the protein, and thus prevent it from reaching the surface of the vesicles, prior to the interaction of the transmembrane helices with the lipids.

In summary, the results herein support the involvement of both helix-1 and helix-2 in the toxic mechanism of Bti toxin. Both these hydrophobic helical segments may facilitate pore formation by the toxin, with a predominant contribution by helix-2. Two protein–protein interaction steps are probably essential for Bti toxin activity: (i) the association between Bti toxin molecules to form the intermolecular aggregate that was described by Maddrell et al. (1989); (ii) the specific assembly of α-helices from several monomers to form a pore.

REFERENCES

Andreu, D., Merrifield, R. B., Steiner, H., & Boman, H. G. (1985) *Biochemistry 24*, 1683–1688.

Bartlett, G. R. (1959) *J. Biol. Chem. 234*, 466–468.

Ben-Efraim, I., Bach, D., & Shai, Y. (1993) *Biochemistry 32*, 2371–2377.

Beschiaschvili, G., & Seelig, J. (1990) *Biochemistry 29*, 52–58.

Bonifacino, J. S., Suzuki, C. K., & Klausner, R. D. (1990) *Science 247*, 79–82.

Bormann, B. J., Knowles, W. J., & Marchesi, V. T. (1989) *J. Biol. Chem. 264*, 4033–4037.

Chattopadhyay, A., & London, E. (1987) *Biochemistry 26*, 39–45.

Chen, H. C., Brown, J. H., Morell, J. L., & Huang, C. M. (1988) *FEBS Lett. 236*, 461–466.

Chen, Y. H., Yang, J. T., & Chau, K. H. (1974) *Biochemistry 13*, 3350–3359.

Connor, J., & Schroit, A. J. (1987) *Biochemistry 26*, 5099–5105.

Drobniewski, F. A., & Ellar, D. J. (1989) *J. Bacteriol. 171*, 3060–3067.

Earp, D. J., & Ellar, D. J. (1987) *Nucleic Acids Res. 15*, 3619.

Förster, T. (1959) *Faraday Discuss. Chem. Soc. 27*, 7–17.

Frey, S., & Tamm, L. K. (1990) *Biochem. J. 272*, 713–719.

Fung, B. K., & Stryer, L. (1978) *Biochemistry 17*, 5241–5248.

Gazit, E., & Shai, Y. (1993) *Biochemistry 32*, 3429–3436.

Ghosh, P., & Stroud, R. M. (1991) *Biochemistry 30*, 3551–3557.

Gibson, B. W., Poulter, L., Williams, D. H., & Maggio, J. E. (1986) *J. Biol. Chem. 261*, 5341–5349.

Gill, S. S., Singh, G. J., & Hornung, J. M. (1987) *Infect. Immun. 55*, 1300–1308.

Gill, S. S., Cowles, E. A., & Pietrantonio, P. V. (1992) *Annu. Rev. Entomol. 37*, 615–636.

Goldberg, L. J. & Margalit, J. (1977) *Mosq. News 37*, 355–358.

Greenblatt, R. E., Blatt, Y. & Montal, M. (1985) *FEBS Lett. 193*, 125–134.

Grove, A., Tomich, J. M., & Montal, M. (1991) *Proc. Natl. Acad. Sci. U.S.A. 88*, 6418–6422.

Guy, H. R., & Seetharamulu, P. (1986) *Proc. Natl. Acad. Sci. U.S.A. 83*, 508–512.

Höfte, H., & Whiteley, H. R. (1989) *Microbiol. Rev. 53*, 242–255.

Inouye, M. (1974) *Proc. Natl. Acad. Sci. U.S.A. 71*, 2396–2400.

Kahn, T. W., & Engelman, D. M. (1992) *Biochemistry 31*, 6144–6151.

Kenner, R. A., & Aboderin, A. A. (1971) *Biochemistry 10*, 4433–4440.

Knowles, B. H., Blatt, M. R., Tester, M., Horsnell, J. M., Carroll, J., Menestrina, G., & Ellar, D. J. (1989) *FEBS Lett. 244*, 259–262.

Langosch, D., Hartung, K., Grell, E., Bamberg, E., & Betz, H. (1991) *Biochim. Biophys. Acta 1063*, 36–44.

Lear, J. D., Wasserman, Z. R., & DeGrado, W. F. (1988) *Science 240*, 1177–1181.

Lemmon, M. A., & Engelman, D. M. (1992) *Curr. Opin. Struct. Biol. 2*, 511–518.

Lemmon, M. A., Flanagan, J. M., Hunt, J. F., Adair, B. D., Bormann, B. J., Dempsey, C. E., & Engelman, D. M. (1992) *J. Biol. Chem. 267*, 7683–7689.

Loew, L. M., Rosenberg, I., Bridge, M., & Gitler, C. (1983) *Biochemistry 22*, 837–844.

Lynch, B. A., & Koshland, D. E., Jr. (1991) *Proc. Natl. Acad. Sci. U.S.A. 88*, 10402–10406.

Maddrell, S. H., Overton, J. A., Ellar, D. J., & Knowles, B. H. (1989) *J. Cell Sci. 94*, 601–608.

Manolios, N., Bonifacino, J. S., & Klausner, R. D. (1990) *Science 249*, 274–277.

Mao, D., & Wallace, B. A. (1984) *Biochemistry 23*, 2667–2673.

Merrifield, R. B., Vizioli, L. D., & Boman, H. G. (1982) *Biochemistry 21*, 5020–5031.

Mor, A., Nguyen, V. H., Delfour, A., Migliore, S. D., & Nicolas, P. (1991) *Biochemistry 30*, 8824–8830.

Oiki, S., Danho, W., Madison, V., & Montal, M. (1988) *Proc. Natl. Acad. Sci. U.S.A. 85*, 8703–8707.

Papahadjopoulos, D., & Miller, N. (1967) *Biochim. Biophys. Acta 135*, 624–638.

Popot, J.-L., & Engelman, D. M. (1990) *Biochemistry 29*, 4031–4037.

Popot, J.-L., Gerchman, S.-E., & Engelman, D. M. (1987) *J. Mol. Biol. 198*, 655–676.

Pouny, Y., & Shai, Y. (1992) *Biochemistry 31*, 9482–9490.
Pouny, Y., Rapaport, D., Mor, A., Nicolas, P., & Shai, Y. (1992) *Biochemistry 31*, 12416–12423.
Rajarathnam, K., Hochman, J., Schindler, M., & Ferguson, M. S. (1989) *Biochemistry 28*, 3168–3176.
Rapaport, D., & Shai, Y. (1991) *J. Biol. Chem. 266*, 23769–23775.
Rapaport, D., & Shai, Y. (1992) *J. Biol. Chem. 267*, 6502–6509.
Rapaport, D., Danin, M., Gazit, E., & Shai, Y. (1992) *Biochemistry 31*, 8868–8875.
Rizzo, V., Stankowski, S., & Schwarz, G. (1987) *Biochemistry 26*, 2751–2759.
Schiffer, M. & Edmunson, A. B. (1967) *Biophys. J. 7*, 121–135.
Schwarz, G., Gerke, H., Rizzo, V., & Stankowsky, S. (1987) *Biophys. J. 52*, 685–692.
Shai, Y., Bach, D., & Yanovsky, A. (1990) *J. Biol. Chem. 265*, 20202–20209.
Shai, Y., Hadari, Y. R., & Finkels, A. (1991) *J. Biol. Chem. 266*, 22346–22354.
Sims, P. J., Waggoner, A. S., Wang, C. H., & Hoffmann, J. R. (1974) *Biochemistry 13*, 3315–3330.
Stankowski, S., & Schwarz, G. (1990) *Biochim. Biophys. Acta 1025*, 164–172.
Sternberg, M. J. E., & Gullick, W. J. (1990) *Protein Eng. 3*, 245–248.
Thiaudière, E., Siffert, O., Talbot, J. C., Bolard, J., Alouf, J. E., & Dufourcq, J. (1991) *Eur. J. Biochem. 195*, 203–213.
Thomas, W. E., & Ellar, D. J. (1983) *FEBS Lett. 154*, 362–368.
Tosteson, M. T., Auld, D. S., & Tosteson, D. C. (1989) *Proc. Natl. Acad. Sci. U.S.A. 86*, 707–710.
Vogel, H., & Jahnig, F. (1986) *Biophys. J. 50*, 573–582.
Waalwijk, C., Dullemans, A. M., van Workum, M. E. S., & Visser, B. (1985) *Nucleic Acids Res. 13*, 8207–8217.
Ward, E. S., & Ellar, D. J. (1986) *J. Mol. Biol. 191*, 1–11.
Ward, E. S., Ellar, D. J., & Chilcott, C. N. (1988) *J. Mol. Biol. 202*, 527–535.
Wu, C. S. C., Ikeda, K., & Yang, J. T. (1981) *Biochemistry 20*, 566–570.